Manuscript Details

Manuscript number	TWST_2017_1027
Title	Flexural behavior of steel deep beams prestressed with externally unbonded straight multi-tendons
Article type	Research Paper

Abstract

External prestressing is one of the most powerful techniques to retrofit and strengthen the existing beams and columns. In this paper, the flexural behavior of deep beam prestressed with multi-tendons is investigated under concentrated forces for both post- and pre- tensioning process. Solutions for displacements and stresses are achieved based on Timoshenko beam theory. Besides, a statically indeterminate system was established, and a compatibility condition between the beam and tendons was founded to solve the increase in tendon force in loading period in pre-tensioning. Verifications were performed in tables by applying Finite element analysis. Finally, parameter studies were carried out to examine the effects of tendon force and eccentricity on the flexure of beams. Numerical results were summarized into a series of curves indicating the distribution of warping stresses on flanges and the increases in sub-tendon forces.

Manuscript region of origin	China

Corresponding Author	Yangzhi Ren
Corresponding Author's Institution	Key Lab of Civil Engineering Safety and Durability of China Education Ministry, Department of Civil Engineering
Order of Authors	Yangzhi Ren, yuanqing wang, Bin Wang, Huiyong Ban, Jia Song, Gang Su

Submission Files Included in this PDF

File Name [File Type]

cover letter.docx [Cover Letter]

highlights.docx [Highlights]

manuscript.pdf [Manuscript File]

To view all the submission files, including those not included in the PDF, click on the manuscript title on your EVISE Homepage, then click 'Download zip file'.

Dear Editor:

We would like to submit the manuscript entitiled "*Flexural behavior of steel deep beams prestressed with externally unbonded straight multi-tendons*" to **Thin-Walled Structures**. This is an original paper. Neither the entire paper nor any part of its content has been published or accepted elsewhere. It is not being submitted to any other journal. I have read and have abided by the statement of ethical standards for manuscripts submitted to **Thin-Walled Structures**. All authors have seen the manuscript and approved to submit to your journal.

This paper presents the flexural behavior of deep beams prestressed with multi-tendons under concentrated forces for both post- and pre- tensioning processes. Solutions for displacements and stresses are obtained based on Timoshenko beam theory. Verifications and Parameter studies were performed successively later in the paper.

I look forward to hearing from you in due course.
Yours Sincerely.

Yangzhi Ren
On behalf of all other coauthors

1. Flexural behavior of deep beam prestressed with multi-tendons is analyzed for both post- and pre- tensioning processes.

2. Solutions for displacements and stresses are obtained based on Timoshenko beam theory.

3. The compatibility condition between beam and tendons needs to be found to solve the increase in tendon force.

4. The proposed method is capable of estimating the displacements, stresses and the increase in tendon force.

Flexural behavior of steel deep beams prestressed with externally unbonded straight multi-tendons

Yangzhi Ren[a*], Yuanqing Wang[a], Bin Wang[b], Huiyong Ban[a], Jia Song[c], Gang Su[d]

[a] Key Lab of Civil Engineering Safety and Durability of China Education Ministry, Department of Civil Engineering, Tsinghua University, Beijing, China, 100084.
[b] College of Engineering, Design and Physical Sciences, Brunel University, London, Uxbridge UB8 3PH, UK.
[c] Beijing Building Construction Research Institute co.,Ltd., Beijing, China, 100039
[d] Shanghai Boiler Works co., Ltd., Shanghai, China, 200245
[*]:Corresponding author, e-mail address: renyz66@mail.tsinghua.edu.cn

Abstract: External prestressing is one of the most powerful techniques to retrofit and strengthen the existing beams and columns. In this paper, the flexural behavior of deep beam prestressed with multi-tendons is investigated under concentrated forces for both post- and pre- tensioning processes. Solutions for displacements and stresses are achieved based on Timoshenko beam theory. Besides, a statically indeterminate system was established, and a compatibility condition between the beam and tendons was founded to solve the increase in tendon force in loading period in pre-tensioning. Verifications were performed in tables by applying Finite element analysis. Finally, parameter studies were carried out to examine the effects of tendon force and eccentricity on the flexure of beams. Numerical results were summarized into a series of curves indicating the distribution of warping stresses on flanges and the increases in sub-tendon forces.

Keywords: Prestressed deep beam; Multi-tendons; Post-tensioning; Pre-tensioning; Compatibility condition

1. Introduction

Steel deep beams with large height-to-span ratio are widely used in buildings and offshore structures. As shown in Fig.1, a series of steel large plate girders (deep beams) are applied to resist the external loads from boiler in electric power plant. Due to the overloading, many girders are suffering from fatigue and fracture problems, and are in need of rehabilitation and replacement.

Externally prestressed technique is an effective way to retrofit existing beams, which produces additional stresses in the direction that opposes to the external loads [1-2]. Externally prestressed beams possess many advantages such as large loading capacity [3], favorable fatigue and fracture behaviors [4], full use of materials and structural lightweight [5], ease in inspection and replacement of tendons [6], high redundancy and reliability [7-8].

Different from the internally prestressed tendons in concrete, externally prestressed tendons are located outside the beam and are fixed between anchorages. Therefore, tendons are free to move with respect to the beam axis, resulting in a gradual variation in tendon eccentricity [9-10].

Although researches on the externally prestressed technique has been mature in concrete beams [10-13], composite steel-concrete beams [1-8, 14-17] and concrete deep beams [18-20], those on prestressed steel deep beams are still scarce. More recently, Belletti [21] investigated the flexure of prestressed I-shaped steel beams and found that more deviators result in the higher prestressed force and more stability of beams. Park [22] found that the flexural capacity increased by 30% to 40% for beams prestressed with straight tendons, and even higher for those with draped tendons. Besides, researches on the continuous steel beams prestressed with external tendons show that the increase of the height of cross section at internal supports effectively reduces the deflections and stresses induced by negative moments [23]. Further, the externally prestressed technique increases the torsional stability of beams, and the capacity increases along with the eccentricity of tendons [24].

(a) electric power plant (b) large plate girders

Fig.1 Large plate girders in electric power plant

A detail observation on the literatures reveals that most researches generally focus on the prestressed beams with only one straight/draped tendon, but less on those with multi-tendons. This motivates the author to investigate the flexural behavior of deep beams with multi-tendons. In this paper, formulas for displacements and stresses were obtained for steel deep beams prestressed with multi-tendons for both post- and pre- tensioning processes. A high-order indeterminate system was established in loading period in pre-tensioning, and the compatibility between the beam and tendons was found to solve the increase in tendon force. Finite element analysis was applied to verify the accuracy of the proposed method for both tensioning processes. Finally, parameter studies were performed to investigate the effects of tendon force and eccentricity on the flexural behavior of prestressed beams with multi-tendons.

2. Structural model

For analysis, a orthogonal coordinate system O-xyz is established in Fig.2. The I-shaped beam is made of a homogenous, isotropic and elastic steel with Young's and shear moduli E and G. The span is l. The height and width of the cross section are h and b. The thicknesses of top and bottom flanges are uniform t_{f} and the thickness of web is t_{w}, respectively. The concentrated forces P_is (i=1, 2, …n) are acted on the centroid axis in the symmetrical plane XY, having a distance of c_i away from the right end of the beam. The uniform load q represents the beam self weight, having '$q=\rho Ag$', where ρ is the density, A is the cross-sectional area of the beam, g is the acceleration of y-axial gravity. u and v are horizontal and vertical displacements, respectively.

The tendons T_j (j=1, 2, …, k), with the eccentricities of e_j away from the x-axis, are anchored between endplates, introducing a negative moment to resist the deformations produced by P_i and q. Tendons are equally divided into two sub-tendons (Fig.2b), being symmetrical with respect to the plane XY. The elastic modulus and cross-sectional area are indicated by $E_{\mathrm{T}j}$ and $A_{\mathrm{T}j}$ for the sub-tendons at the jth row, respectively.

In following analysis, each couple of sub-tendons at the same height is regarded as one single tendon with its path through the plane XY. Besides, all forces in tendons are effective without involving the prestressing loss. The self weight of tendons and the deflection of tendons due to self weight are not considered, so all tendons keep straight during the tensioning process.

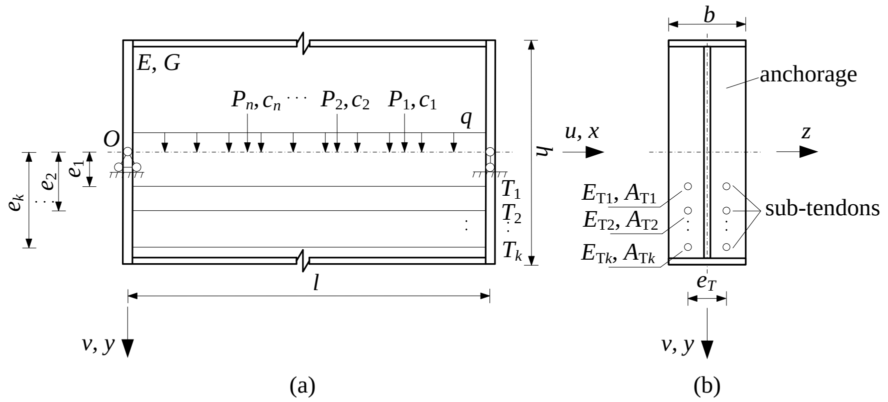

Fig.2 Deep beams prestressed with straight unbonded multi-tendons

According to the application sequence of external forces P_i and the prestressed forces S_j, the tensioning process is classified into post-tensioning and pre-tensioning. For post-tensioning, two periods are performed in sequence in Fig.3. The prestressed forces S_j are applied after P_i, resulting in the reduction of downward deformation induced by P_i and q. While for pre-tensioning, as shown in Fig.4, the initial prestressed forces S_{0j} are applied before P_i, resulting in a upward deflection in prestressing period. Then a high-order statically indeterminate system is established later in loading period, producing an extra increase $S_{\Delta j}$ in each tendon T_j due to P_i.

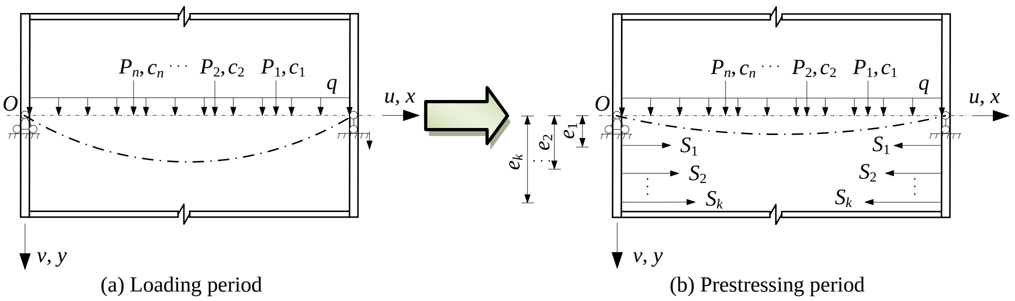

Fig.3 Post-tensioning

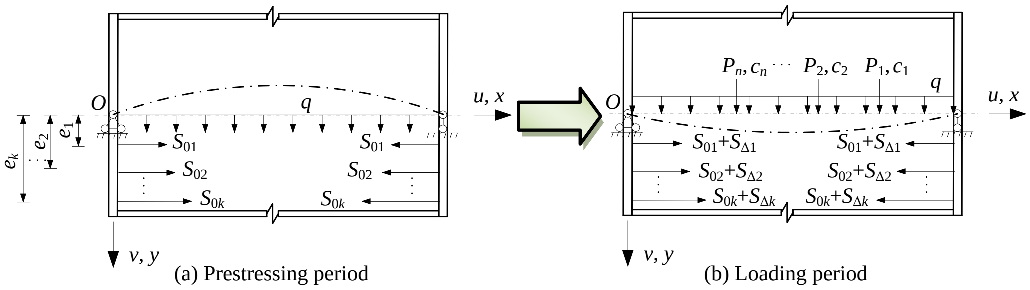

Fig.4 Pre-tensioning

Actually, there is another case that the prestressed forces S_{0j} cannot overcome the self weight q and the beam still displays downwards in prestressing period in pre-tensioning. However, this can be regarded as a special case in prestressing period in post-tensioning, where $P_i=0$. So only the upward case is studied in prestressing period in pre-tensioning.

In the following, the displacements and stresses for both tensioning processes are analyzed respectively.

3. Post-tensioning

For post-tensioning, two periods are performed in sequence.

3.1. Loading period

Based on Timoshenko beam theory [25], the moment equation due to the self weight q is

$$EI\frac{\mathrm{d}^2\left[{}^1v_q(x)\right]}{\mathrm{d}x^2}=-\frac{qlx}{2}+\frac{qx^2}{2}-\frac{EI\alpha_\mathrm{s}q}{GA} \tag{1}$$

where ${}^1v_q(x)$ is the y-axial displacement due to q in loading period. I is the moment of inertia of the beam section with respect to z-axis. A is the cross-sectional area of the beam. α_s is the shear stress distribution coefficient, $\alpha_\mathrm{s}=A/A_\mathrm{w}$ for I-shaped beam, A_w is the web area of the beam, $A_\mathrm{w}=t_\mathrm{w}(h\text{-}2t_\mathrm{f})$.

For simply supported beam, the solution for Eq.(1) is

$${}^1v_q(x)=\frac{qx}{24EI}\left(l^3-2lx^2+x^3\right)+\frac{\alpha_\mathrm{s}q}{2GA}x\left(l-x\right) \tag{2}$$

The displacements due to P_i are obtained in the form of piecewise function [25]

$${}^1v_{Pi}(x)=\frac{P_ic_ix\left(l^2-x^2-c_i^2\right)}{6EIl}+\frac{\alpha_\mathrm{s}P_ic_i}{GAl}x\text{, for }0\le x\le l\text{-}c_i \tag{3}$$

$${}^1v_{Pi}(x)=\frac{1}{6EIl}\left[P_il\left(x-l+c_i\right)^3+P_ic_ix\left(l^2-c_i^2\right)-P_ic_ix^3\right]+\frac{\alpha_\mathrm{s}P_i}{GAl}\left(l-c_i\right)\left(l-x\right)\text{, for }l\text{-}c_i\le x\le l \tag{4}$$

If we assume there are m of n forces (P_1, P_2, .., P_m) located at the right of calculated point x, then the total displacement caused by all P_is can be obtained by superimposing Eq.(3) for forces P_1, P_2, .., P_m and Eq.(4) for forces P_{m+1}, P_{m+2}, …, P_n.

$$\begin{aligned}{}^1v_P(x)=&\frac{x}{6EIl}\sum_{i=1}^{m}P_ic_i\left(l^2-x^2-c_i^2\right)+\frac{\alpha_\mathrm{s}x}{GAl}\sum_{i=1}^{m}P_ic_i\\&+\frac{1}{6EIl}\sum_{i=m+1}^{n}\left[P_il\left(x-l+c_i\right)^3+P_ic_ix\left(l^2-c_i^2\right)-P_ic_ix^3\right]+\frac{\alpha_\mathrm{s}\left(l-x\right)}{GAl}\sum_{i=m+1}^{n}P_i\left(l-c_i\right)\end{aligned} \tag{5}$$

Combining Eq.(2) with Eq.(5), the total displacement in loading period is

$$\begin{aligned}{}^1v(x)=&\frac{qx}{24EI}\left(l^3-2lx^2+x^3\right)+\frac{\alpha_\mathrm{s}qx}{2GA}\left(l-x\right)+\frac{x}{6EIl}\sum_{i=1}^{m}P_ic_i\left(l^2-x^2-c_i^2\right)+\frac{\alpha_\mathrm{s}x}{GAl}\sum_{i=1}^{m}P_ic_i\\&+\frac{1}{6EIl}\sum_{i=m+1}^{n}\left[P_il\left(x-l+c_i\right)^3+P_ic_ix\left(l^2-c_i^2\right)-P_ic_ix^3\right]+\frac{\alpha_\mathrm{s}\left(l-x\right)}{GAl}\sum_{i=m+1}^{n}P_i\left(l-c_i\right)\end{aligned} \tag{6}$$

Correspondingly, the warping stress is

$${}^1\sigma_x(x,y)=-\frac{y}{Il}\left[\frac{qxl\left(x-l\right)}{2}-x\sum_{i=1}^{m}P_ic_i+\sum_{i=m+1}^{n}P_i\left(l-c_i\right)\left(x-l\right)\right]+\frac{E\alpha_\mathrm{s}qy}{GA} \tag{7}$$

3.2. Prestressing period

Referred to Fig.5, the moment equation due to q in prestressing period is

$$EI\frac{\mathrm{d}^2\left[{}^2v_q(x)\right]}{\mathrm{d}x^2}=-{}^2v_q(x)\sum_{j=1}^{k}S_j-\frac{qlx}{2}+\frac{qx^2}{2}-\frac{EI\alpha_\mathrm{s}q}{GA}+\sum_{j=1}^{k}M_j \tag{8}$$

where ${}^2v_q(x)$ is the y-axial displacement due to q in prestressing period. M_j is the ending moment due to the prestressed force S_j, M_j=S_je_j. S_j and e_j are the prestressed force and eccentricity of the jth tendon (j=1,2,…,k), see Fig.3b.

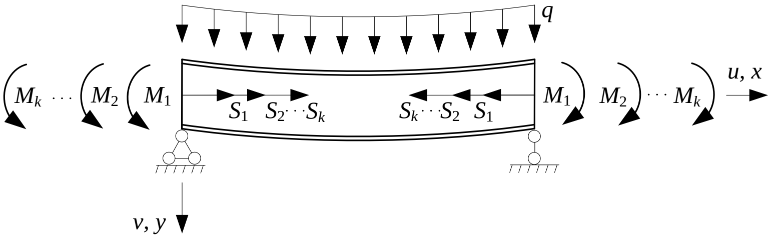

Fig.5 Model of prestressed deep beams in prestressing period in post-tensioning

For simply supported beam, the solution for Eq.(8) is

$$ {}^2v_q(x)=\left(\frac{\alpha_s q}{GAp^2}+\frac{q}{EIp^4}-\frac{1}{EIp^2}\sum_{j=1}^{k}S_je_j\right)\left[\frac{1}{\cos\frac{pl}{2}}\cos p\left(\frac{l}{2}-x\right)-1\right]+\frac{qx^2}{2EIp^2}-\frac{qlx}{2EIp^2} \quad (9)$$

where $p^2=\frac{1}{EI}\sum_{j=1}^{k}S_j$.

The moment equation due to P_i is

$$EI\frac{\mathrm{d}^2\left[{}^2v_{Pi}(x)\right]}{\mathrm{d}x^2}=-{}^2v_{Pi}(x)\sum_{j=1}^{k}S_j-\frac{P_ic_ix}{l}\text{, for } 0\le x\le l-c_i \quad (10)$$

$$EI\frac{\mathrm{d}^2\left[{}^2v_{Pi}(x)\right]}{\mathrm{d}x^2}=-{}^2v_{Pi}(x)\sum_{j=1}^{k}S_j-\frac{P_i}{l}\left(l-c_i\right)\left(l-x\right)\text{, for } l-c_i\le x\le l \quad (11)$$

where ${}^2v_{Pi}(x)$ is the displacement due to P_i without shear effect.

For simply supported beam, the solutions for Eq.(10) and Eq.(11) are

$${}^2v_{Pi}(x)=\frac{P_i\sin pc_i\sin px}{EIp^3\sin pl}-\frac{P_ic_ix}{EIlp^2}\text{, for } 0\le x\le l-c_i \quad (12)$$

$${}^2v_{Pi}(x)=\frac{P_i\sin p\left(l-c_i\right)}{EIp^3\sin pl}\sin p\left(l-x\right)-\frac{P_i\left(l-c_i\right)\left(l-x\right)}{EIlp^2}\text{, for } l-c_i\le x\le l \quad (13)$$

Referred to Eq.(3) and Eq.(4), the displacements due to P_i with shear effect are

$${}^2v_{Pi}(x)=\frac{P_i\sin pc_i\sin px}{EIp^3\sin pl}+\frac{P_ic_ix}{l}\left(\frac{\alpha_s}{GA}-\frac{1}{EIp^2}\right)\text{, for } 0\le x\le l-c_i \quad (14)$$

$${}^2v_{Pi}(x)=\frac{P_i\sin p\left(l-c_i\right)}{EIp^3\sin pl}\sin p\left(l-x\right)+\frac{P_i\left(l-c_i\right)\left(l-x\right)}{l}\left(\frac{\alpha_s}{GA}-\frac{1}{EIp^2}\right)\text{, for } l-c_i\le x\le l \quad (15)$$

Referred to Eq.(5), the displacement due to all P_is can be obtained by superimposing Eq.(14) for forces P_1, P_2, .., P_m and Eq.(15) for forces P_{m+1}, P_{m+2}, …, P_n. Therefore, the total y-axial displacement in prestressing period is

$$
{}^2v(x)=\left(\frac{\alpha_s q}{GAp^2}+\frac{q}{EIp^4}-\frac{1}{EIp^2}\sum_{j=1}^{k}S_j e_j\right)\left[\frac{1}{\cos\frac{pl}{2}}\cos p\left(\frac{l}{2}-x\right)-1\right]
+\frac{\sin px}{EIp^3\sin pl}\sum_{i=1}^{m}P_i\sin pc_i+\frac{\sin p(l-x)}{EIp^3\sin pl}\sum_{i=m+1}^{n}P_i\sin p(l-c_i)
+\left(\frac{\alpha_s}{GA}-\frac{1}{EIp^2}\right)\left[\frac{x}{l}\sum_{i=1}^{m}P_i c_i+\frac{l-x}{l}\sum_{i=m+1}^{n}P_i(l-c_i)\right]+\frac{q}{2EIp^2}\left(x^2-lx\right) \tag{16}
$$

Correspondingly, the warping stress is

$$
{}^2\sigma_x(x,y)=Ey\left[\begin{array}{l}\frac{1}{\cos\frac{pl}{2}}\left(\frac{\alpha_s q}{GA}+\frac{q}{EIp^2}-\frac{1}{EI}\sum_{j=1}^{k}S_j e_j\right)\cos p\left(\frac{l}{2}-x\right)-\frac{q}{EIp^2}\\ +\frac{\sin px}{EIp\sin pl}\sum_{i=1}^{m}P_i\sin pc_i+\frac{\sin p(l-x)}{EIp\sin pl}\sum_{i=m+1}^{n}P_i\sin p(l-c_i)\end{array}\right]-\frac{\sum_{j=1}^{k}S_j}{A} \tag{17}
$$

4. Pre-tensioning

4.1. Prestressing period

Referred to Fig.6, the moment equation due to q in prestressing period is

$$
EI\frac{\mathrm{d}^2\left[{}^3v(x)\right]}{\mathrm{d}x^2}={}^3v(x)\sum_{j=1}^{k}S_{0j}-\frac{qlx}{2}+\frac{qx^2}{2}-\frac{EI\alpha_s q}{GA}+\sum_{j=1}^{k}M_{0j} \tag{18}
$$

where ${}^3v(x)$ is the y-axial displacement in prestressing period. M_{0j} is the ending moment, $M_{0j}=S_{0j}e_j$. S_{0j} is the initial prestressed force of the tendon T_j (j=1, 2,…, k), see Fig.4a.

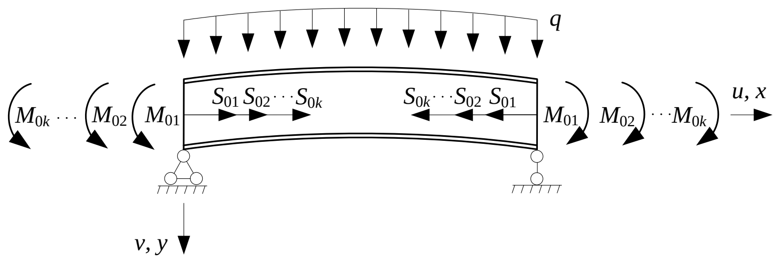

Fig.6 Model of prestressed deep beams in prestressing period in pre-tensioning

For simply supported beam, the solution for Eq.(18) is

$$
{}^3v(x)=\left(\frac{\alpha_s q}{GAp_0^2}-\frac{q}{EIp_0^4}-\frac{1}{EIp_0^2}\sum_{j=1}^{k}S_{0j}e_j\right)\left[1-\frac{\cosh p_0\left(x-\frac{l}{2}\right)}{\cosh\frac{p_0 l}{2}}\right]-\frac{qx^2}{2EIp_0^2}+\frac{qlx}{2EIp_0^2} \tag{19}
$$

where $p_0^2=\frac{1}{EI}\sum_{j=1}^{k}S_{0j}$.

Correspondingly, the warping stress is

$$
{}^3\sigma_x(x,y)=\frac{y}{I\cosh\frac{p_0 l}{2}}\left(\frac{EI\alpha_s q}{GA}-\sum_{j=1}^{k}S_{0j}e_j-\frac{q}{p_0^2}\right)\cosh p_0\left(x-\frac{l}{2}\right)+\frac{yq}{p_0^2 I}-\frac{1}{A}\sum_{j=1}^{k}S_{0j} \tag{20}
$$

4.2. Loading period

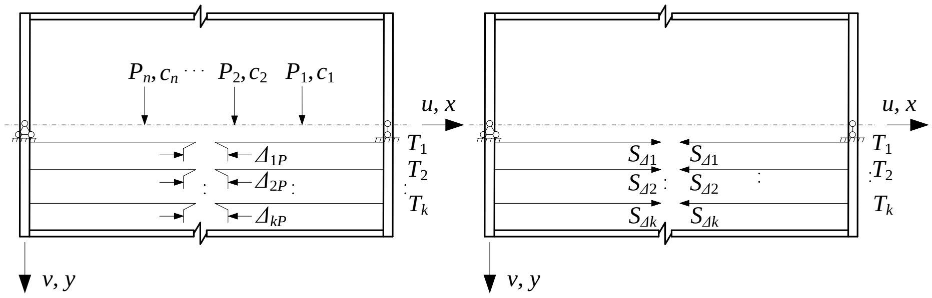

(a) gaps Δ_{jP} produced by P_i (b) the increase $S_{\Delta j}$ in tendon force

Fig.7 Statically indeterminate system

In this period, a high-order indeterminate system is established including both the beam and tendons, producing an increase $S_{\Delta j}$ (j=1,2,…,k) in tendon T_j , as shown in Fig.4b. The key point of solving $S_{\Delta j}$ is to find the compatibility condition between the beam and tendons. To do this, a scenario is configured in Fig.7, where all tendons are frictionally cut off. The gap between cutting sections enlarges due to P_is (Fig.7a) and shortens due to $S_{\Delta j}$ (Fig.7b). Therefore, the compatibility equation is

$$\begin{bmatrix} \delta_{11} & \delta_{12} & \cdots & \delta_{1k} \\ \delta_{21} & \delta_{22} & \cdots & \delta_{2k} \\ \cdots & \cdots & & \cdots \\ \delta_{k1} & \delta_{k2} & & \delta_{kk} \end{bmatrix} \begin{Bmatrix} S_{\Delta 1} \\ S_{\Delta 2} \\ \cdots \\ S_{\Delta k} \end{Bmatrix} + \begin{Bmatrix} \Delta_{1P} \\ \Delta_{2P} \\ \cdots \\ \Delta_{kP} \end{Bmatrix} = \begin{Bmatrix} 0 \\ 0 \\ \cdots \\ 0 \end{Bmatrix} \tag{21}$$

where Δ_{jP} is the gap length due to P_is. δ_{rs} is the rth gap length due to the unit prestressed force in the sth tendon (r, s =1, 2, …, k). Based on the virtual work theory, Δ_{jP} and δ_{rs} are

$$\Delta_{jP} = \int_0^l \frac{\bar{M}_j(x) M_P(x)}{EI} \mathrm{d}x + \alpha_s \int_0^l \frac{\bar{Q}_j(x) Q_P(x)}{GA} \mathrm{d}x \tag{22}$$

$$\delta_{rs} = \begin{cases} \int_0^l \frac{\bar{M}_r(x)\bar{M}_s(x)}{EI} \mathrm{d}x + \int_0^l \frac{\bar{S}_r(x)\bar{S}_s(x)}{EA} \mathrm{d}x + \alpha_s \int_0^l \frac{\bar{Q}_r(x)\bar{Q}_s(x)}{GA} \mathrm{d}x, & \text{for } r \neq s \\ \int_0^l \frac{\bar{M}_r^2(x)}{EI} \mathrm{d}x + \int_0^l \frac{\bar{S}_r^2(x)}{EA} \mathrm{d}x + \alpha_s \int_0^l \frac{\bar{Q}_r^2(x)}{GA} \mathrm{d}x + \int_0^l \frac{\bar{S}_r^2(x)}{E_{\mathrm{T}r} A_{\mathrm{T}r}} \mathrm{d}x, & \text{for } r = s \end{cases} \tag{23}$$

where $M_P(x)$ and $Q_P(x)$ are the moment and shear force due to P_is, given by

$$M_P(x) = \frac{x}{l} \sum_{i=1}^{n} P_i c_i - \sum_{i=m+1}^{n} P_i \left(x - l + c_i \right) \tag{24}$$

$$Q_P(x) = \frac{1}{l} \sum_{i=1}^{n} P_i c_i - \sum_{i=m+1}^{n} P_i \tag{25}$$

where m is the number of P_is on the right side of calculation point x. n is the total number of P_is.

$\bar{S}_{r/s}(x)$ are the unit prestressed force in the r/sth tendons, and $\bar{S}_{r/s}(x) = 1$.

$\overline{M}_{j/r/s}(x)$, $\bar{Q}_{j/r/s}(x)$ are the moments and shear forces due to the unit prestressed forces in the j/r/sth tendons, respectively. Therefore, the moment equation due to the unit prestressed force is

$$EI \frac{\mathrm{d}^2 (v_{\mathrm{u}j}(x))}{\mathrm{d}x^2} = v_{\mathrm{u}j}(x) + e_j \tag{26}$$

where $v_{uj}(x)$ is the y-axial displacement due to the unit prestressed force in the jth tendon.

For simply supported beam, the solution for Eq.(26) is

$$v_{uj}(x)=e_j\left[\frac{1}{\cosh\frac{p_u l}{2}}\cosh p_u\left(x-\frac{l}{2}\right)-1\right] \tag{27}$$

where p_u=1/EI.

Therefore, the moment and shear force are

$$\overline{M}_j(x)=-EI\frac{\mathrm{d}^2 v_{uj}(x)}{\mathrm{d}x^2}=-\frac{e_j}{\cosh\frac{p_u l}{2}}\cosh p_u\left(x-\frac{l}{2}\right) \tag{28}$$

$$\overline{Q}_j(x)=\frac{\mathrm{d}\overline{M}_j(x)}{\mathrm{d}x}=\frac{p_u e_j}{\cosh\frac{p_u l}{2}}\sinh p_u\left(\frac{l}{2}-x\right) \tag{29}$$

Similarly, the moments $\overline{M}_{r/s}(x)$ and shear forces $\overline{Q}_{r/s}(x)$ can be obtained by substituting the subscript j with r and s in Eq.(28) and Eq.(29).

Substitute Eqs.(24), (25), (28) and (29) into Eq.(22), and the gap length $\varDelta_{jP}$ is

$$\Delta_{jP}=\frac{e_j}{l\cosh\frac{p_u l}{2}}\sum_{m=0}^{n}\sum_{i=1}^{n}P_i c_i \varPhi_m-\frac{e_j}{\cosh\frac{p_u l}{2}}\sum_{m=0}^{n}\sum_{i=m+1}^{n}P_i\left[p_u\left(l-c_i\right)U_m+\varPhi_m\right] \tag{30}$$

where $\varPhi_m=\frac{\alpha_s}{GA}Z_m-p_u R_m$. R_m, U_m and Z_m represent the first-order difference of functions $R(\beta)$, $U(\beta)$ and $Z(\beta)$ respectively, given by

$$U_m=U(c_{m+1})-U(c_m),\quad U(\beta)=\sinh p_u\left(\beta-\frac{l}{2}\right),$$

$$Z_m=Z(c_{m+1})-Z(c_m),\quad Z(\beta)=\cosh p_u\left(\beta-\frac{l}{2}\right),$$

$$R_m=R(c_{m+1})-R(c_m),\quad R(\beta)=\left(l-\beta\right)U(x)+\frac{Z(\beta)}{p_u}.$$

where c_i (i=1, 2, …, n) is the distance away from the right end of the beam for the force P_i. Plus, c_0=0 and c_{n+1}=l.

Similarly, the gap δ_{rs} in Eq.(23) is

$$\delta_{rs}=\begin{cases}\dfrac{p_u e_r e_s\left(p_u l+\sinh p_u l\right)}{1+\cosh p_u l}\left(1+\dfrac{\alpha_s}{GA}\right)-\dfrac{2\alpha_s l p_u^2 e_r e_s}{GA\left(1+\cosh p_u l\right)}+\dfrac{l}{EA}, & \text{for } r\neq s\\ \dfrac{p_u e_r^2\left(p_u l+\sinh p_u l\right)}{1+\cosh p_u l}\left(1+\dfrac{\alpha_s}{GA}\right)-\dfrac{2\alpha_s l p_u^2 e_r^2}{GA\left(1+\cosh p_u l\right)}+\dfrac{l}{EA}+\dfrac{l}{2E_{Tr}A_{Tr}}, & \text{for } r=s\end{cases} \tag{31}$$

where e_r and e_s are the eccentricities of the rth and sth tendons, respectively. A_{Tr} and E_{Tr} are the cross-sectional area and elastic modular of sub-tendons at the rth row, respectively.

Finally, the increase $S_{\varDelta j}$ in Eq.(21) can be obtained according to Eqs.(30) and (31). Then, substituting the force S_j with the total force 'S_{0j}+$S_{\varDelta j}$', the displacements and stresses in loading period in pre-tensioning are obtained from Eqs.(16) and (17). Plus, it is seen from the Eq.(21) that the increases $S_{\varDelta j}$ has nothing to do with the initial tendon forces S_{0j} and the self weight q.

5. Numerical verification

In order to verify the proposed method, an I-shaped large plate girder (see Fig.1b), externally prestressed with three/four tendons respectively, are investigated by finite element analysis (FEA) using ANSYS software package.

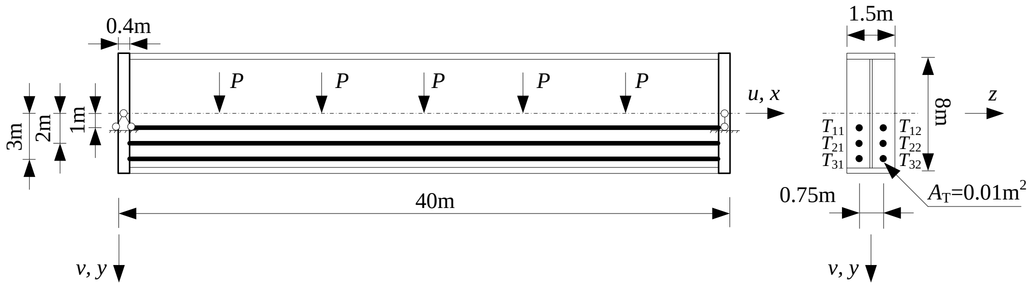

(a) Beams prestressed with three straight tendons

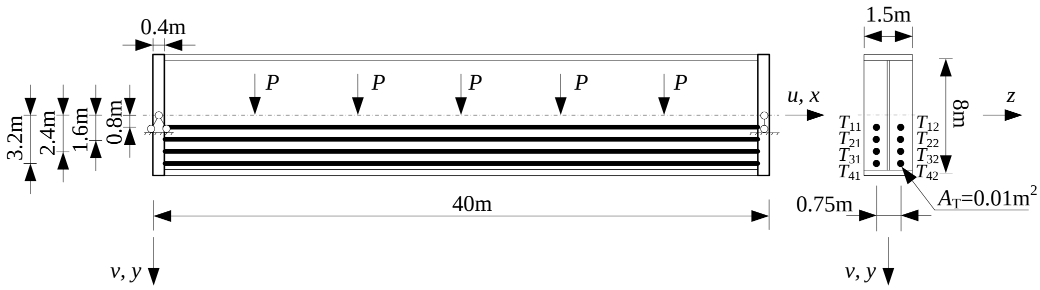

(b) Beams prestressed with four straight tendons

Fig.8 Deep beams prestressed with three (a) and four (b) straight tendons

Measurements

The model is shown in Fig.8 and the measurements are selected from practice.

For beam, the span l is 40m, the height h and width b of the cross section are 8m and 1.5m, the thicknesses of flanges and web are 125mm and 45mm, respectively. So the cross-sectional area A of the beam is 0.7294m^2. The Young's elastic module E is 210GPa and Poisson's ratio v is 0.3. The overall yield strength Y_s is 345MPa.

According to the specification in AISC [26], the beam is a non-compact section and a mass of stiffeners are needed to avoid the local web (or flanges) buckling before overall yielding. However, the stiffeners may influence the distribution of warping stresses, probably resulting in a singularity of the stresses at the connections between the web (or flanges) and stiffeners. So the stiffeners are not considered in the model, and the deformation for beams is controlled within elastic range.

For tendons, the eccentricities are shown in Fig.8. Each tendon is divided into a couple of sub-tendons symmetrical with respect to the plane XY (e.g. $T_1 \rightarrow T_{11}+T_{12}$). The cross-sectional area A_T of sub-tendons is uniform 0.01m^2. The distance between sub-tendons is 0.75m. The Young's elastic module E_T of tendons is 200GPa. The tensioning capacity f_{ptk} of sub-tendons is set to be 1625MPa. The tendons' self weight and initial strain are not considered. The prestressed forces in tendons are realized by dropping temperature, and the thermal expansion coefficient C_T of tendons are set to be constantly 1.19×10^{-5}/℃.

Meshing

In FEA, the element of Shell63 is applied for the beam and endplates, and the element of Link10 is for tendons. The meshing grid is shown in Fig.9. A convergence test shows that a total of 1306 elements are adequate for beams with three tendons and 1432 elements for those with four tendons.

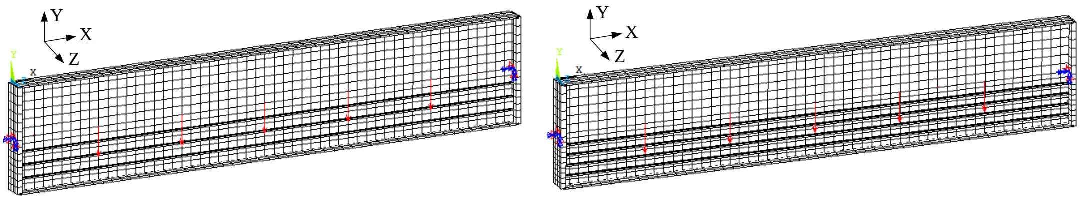

(a) Beams prestressed with three straight tendons (b) Beams prestressed with four straight tendons

Fig.9 Meshing grid

Loadings and constraints

Five concentrated forces P are evenly acted along the centroid axis. The y-axial acceleration g is 9.8N/kg. The density of the beam ρ is 7850 kg/m^3. Therefore, the self-weight q is 56111N/m ($q=\rho Ag$). For simply supported boundary, one end of the beam is hinged and the other is allowed to slide freely on a frictionless support in the direction of x-axis.

5.1. Post-tensioning

In order to verify the deformations and stresses obtained from Eq.(16) and (17), the cases C1 to C11, with a series of tendon forces, are set in Tab.1 for beams with three tendons, and the cases D1 to D11 are in Tab.2 for those with four tendons. f_{ij} is the stress in sub-tendon T_{ij} (i=1,2,3,4; j=1,2), and f_{i1} =f_{i2} due to the symmetry of sub-tendons. The dropping temperatures t_{ij} on the sub-tendons T_{ij} are listed in Tab.3 and Tab.4 respectively for two prestressed beams.

Tab.1 Cases for beams with three tendons

Cases	C1	C2	C3	C4	C5	C6	C7	C8	C9	C10	C11
f_{11} / f_{ptk}	0.35	0.36	0.37	0.38	0.39	0.4	0.41	0.42	0.43	0.44	0.45
f_{21} / f_{ptk}	0.36	0.37	0.38	0.39	0.4	0.41	0.42	0.43	0.44	0.45	0.46
f_{31} / f_{ptk}	0.37	0.38	0.39	0.4	0.41	0.42	0.43	0.44	0.45	0.46	0.47

Tab.2 Cases for beams with four tendons

Cases	D1	D2	D3	D4	D5	D6	D7	D8	D9	D10	D11
f_{11} / f_{ptk}	0.35	0.36	0.37	0.38	0.39	0.4	0.41	0.42	0.43	0.44	0.45
f_{21} / f_{ptk}	0.36	0.37	0.38	0.39	0.4	0.41	0.42	0.43	0.44	0.45	0.46
f_{31} / f_{ptk}	0.37	0.38	0.39	0.4	0.41	0.42	0.43	0.44	0.45	0.46	0.47
f_{41} / f_{ptk}	0.38	0.39	0.4	0.41	0.42	0.43	0.44	0.45	0.46	0.47	0.48

Tab.3 Dropping temperatures on tendons for beams with three tendons in post-tensioning

Cases	C1	C2	C3	C4	C5	C6	C7	C8	C9	C10	C11
t_{11}, t_{12}	-260.7	-268.4	-276.2	-283.9	-291.6	-299.3	-307.0	-314.7	-322.4	-330.1	-337.8
t_{21}, t_{22}	-262.1	-269.9	-277.8	-285.6	-293.4	-301.3	-309.1	-316.9	-324.8	-332.6	-340.4
t_{31}, t_{32}	-257.7	-265.5	-273.3	-281.1	-288.9	-296.7	-304.5	-312.3	-320.1	-327.9	-335.7

Tab.4 Dropping temperatures on tendons for beams with four tendons in post-tensioning

Cases	D1	D2	D3	D4	D5	D6	D7	D8	D9	D10	D11
t_{11}, t_{12}	-271.5	-279.5	-287.4	-295.4	-303.3	-311.3	-319.2	-327.1	-335.1	-343.0	-351.0
t_{21}, t_{22}	-276.5	-284.6	-292.7	-300.8	-308.9	-317.0	-325.1	-333.2	-341.3	-349.4	-357.5
t_{31}, t_{32}	-277.3	-285.5	-293.6	-301.8	-310.0	-318.1	-326.3	-334.4	-342.6	-350.7	-358.9
t_{41}, t_{42}	-273.4	-281.5	-289.6	-297.6	-305.7	-313.8	-321.9	-330.0	-338.1	-346.2	-354.2

It's worth noting that the dropping temperatures in Tab.3 and Tab.4 do not strictly follow the equation 'f_{ij}=$E_T C_T t_{ij}$'. This is because the dropping of temperature on one tendon will not only increase the tensile stress on itself, but also result in the reduction of the stress on the another.

Contours of displacements and stresses are depicted in Fig.10 for non-prestressed beams and two prestressed beams in post-tensioning under the case C6, where P=10000kN. It is seen that the y-axial (vertical) displacements UY at mid span reduce largely from 46.1mm to 29.5mm when prestressed with four straight tendons. The x-axial (warping) stresses SX on bottom flange at mid span reduce largely from 160MPa to 29.9MPa and those on top flange increase slightly from 160MPa to 173MPa after being prestressed, resulting in the downward shift of neutral axis. This infers that the externally prestressed technique can effectively reduce the warping stress on bottom flange and enhance the bending capacity of beam.

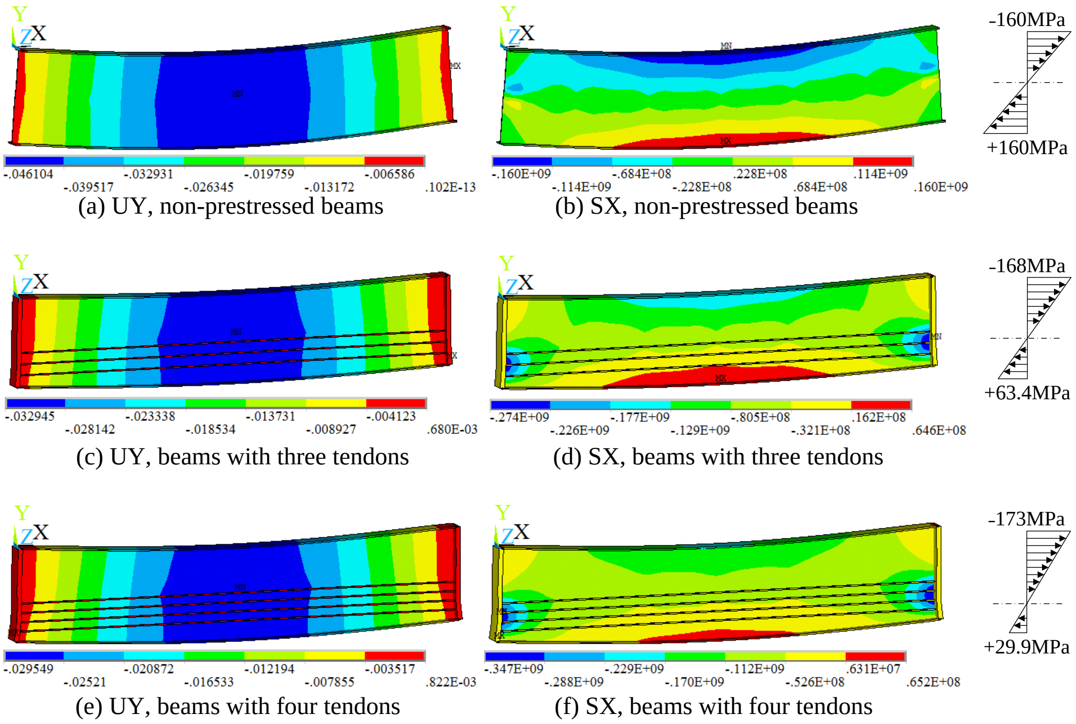

Fig.10 Contours of displacements UY and warping stresses SX for non-prestressed beams and two prestressed beams in post-tensioning under the case C6 (unit: m, Pa).

In post-tensioning, displacements at mid span, obtained from both FEA and the proposed method, are listed in Tab.5 and Tab.6 for two prestressed beams respectively, where P=10000kN. It is obvious that the proposed method (Eq.(16)) provides an acceptable estimation on the y-axial displacements with the relative error (RE) being less than 5% for all cases C1 to C11 and D1 to D11. Therefore, the proposed method is capable of estimating the y-axial displacement for the prestressed beams in post-tensioning.

Tab.5 Comparisons between FEA and the proposed method for the y-axial displacement of beams with three tendons in post-tensioning (unit: mm, direction: downwards)

Cases	C1	C2	C3	C4	C5	C6	C7	C8	C9	C10	C11
FEA	34.10	33.87	33.64	33.41	33.18	32.95	32.72	32.48	32.25	32.02	31.79
Eq.(16)	33.19	32.96	32.72	32.48	32.25	32.01	31.78	31.54	31.30	31.07	30.83
RE (%)	2.66	2.69	2.73	2.76	2.80	2.83	2.87	2.91	2.94	2.98	3.02

Tab.6 Comparisons between FEA and the proposed method for the *y*-axial displacement of beams with four tendons in post-tensioning (unit: mm, direction: downwards)

Cases	D1	D2	D3	D4	D5	D6	D7	D8	D9	D10	D11
FEA	31.09	30.78	30.48	30.17	29.86	29.55	29.24	28.93	28.62	28.31	28.00
Eq.(16)	30.12	29.81	29.49	29.18	28.86	28.54	28.23	27.91	27.60	27.28	26.97
RE (%)	3.12	3.18	3.23	3.28	3.34	3.40	3.46	3.52	3.57	3.63	3.71

Similarly, the warping stresses on flanges at mid span are listed in Tab.7 and Tab.8 for two prestressed beams for two methods, where P=10000kN. It is evident that the proposed method (Eq.(17)) offers an accurate estimation on the warping stresses on flanges with the RE being less than 6% for beams with three tendons. For the warping stresses on bottom flange in Tab.8, though the RE raises up to 16.1% for the case D11, the absolute error (AE) keeps decreasing for the increased tendon forces from D1 to D11. Besides, the warping stresses obtained from Eq.(17) are larger than those from FEA, which proves that the proposed method is conservative. So the proposed method (Eq.(17)) can be applied to estimate the warping stresses on flanges for beams externally prestressesd multi-tendons in post-tensioning.

Tab.7 Comparisons between FEA and the proposed method for warping stresses on flanges for beams with three tendons in post-tensioning (σ_u: stress on top flange, σ_d: stress on bottom flange, unit: MPa)

Cases		C1	C2	C3	C4	C5	C6	C7	C8	C9	C10	C11
σ_u	FEA	-166.3	-166.7	-167.1	-167.4	-167.8	-168.1	-168.5	-168.9	-169.2	-169.6	-169.9
	Eq.(17)	-174.8	-175.1	-175.5	-175.8	-176.1	-176.4	-176.8	-177.1	-177.4	-177.8	-178.1
	RE (%)	4.84	4.81	4.78	4.76	4.73	4.71	4.68	4.65	4.63	4.60	4.58
σ_d	FEA	75.0	72.6	70.3	68.0	65.7	63.4	61.1	58.8	56.4	54.1	51.8
	Eq.(17)	78.5	76.2	73.9	71.5	69.2	66.8	64.5	62.1	59.8	57.5	55.1
	RE (%)	4.57	4.67	4.78	4.90	5.03	5.16	5.30	5.46	5.62	5.80	6.00

Tab.8 Comparisons between FEA and the proposed method for warping stresses on flanges for beams with four tendons in post-tensioning (σ_u: stress on top flange, σ_d: stress on bottom flange, unit: MPa)

Cases		D1	D2	D3	D4	D5	D6	D7	D8	D9	D10	D11
σ_u	FEA	-170.6	-171.1	-171.5	-172.0	-172.5	-173.0	-173.4	-173.9	-174.4	-174.9	-175.4
	Eq.(17)	-178.6	-179.1	-179.5	-180.0	-180.4	-180.8	-181.3	-181.7	-182.1	-182.6	-183.0
	RE (%)	4.51	4.48	4.45	4.41	4.38	4.35	4.31	4.28	4.25	4.22	4.18
σ_d	FEA	45.4	42.3	39.2	36.1	33.0	29.9	26.8	23.7	20.7	17.6	14.5
	Eq.(17)	48.5	45.4	42.3	39.2	36.0	32.9	29.8	26.6	23.5	20.4	17.3
	AE	3.17	3.13	3.09	3.05	3.01	2.97	2.93	2.89	2.86	2.82	2.78
	RE (%)	6.52	6.89	7.31	7.79	8.36	9.04	9.85	10.87	12.14	13.82	16.10

5.2. Pre-tensioning

Similarly, the above cases C1 to C11 and D1 to D11 are both applied to verify accuracy of Eqs.(19) and (20) for prestressed beams in pre-tensioning, where the tendon force refers to the initial prestressed force. The dropping temperatures t_{ij} on the sub-tendons T_{ij} in pre-tensioning are shown in Tab.9 and Tab.10 for two prestressed beams respectively. Similarly, the dropping temperatures do not follow the relation '$f_{ij}=E_T C_T t_{ij}$' due to the interactions between tendons.

Tab.9 Dropping temperatures on tendons for beams with three tendons in pre-tensioning

Cases	C1	C2	C3	C4	C5	C6	C7	C8	C9	C10	C11
t_{11}, t_{12}	-270.4	-278.1	-285.8	-293.5	-301.2	-308.9	-316.6	-324.3	-332.0	-339.8	-347.5
t_{21}, t_{22}	-281.4	-289.3	-297.1	-305.0	-312.8	-320.6	-328.5	-336.3	-344.1	-352.0	-359.8
t_{31}, t_{32}	-287.0	-294.8	-302.6	-310.4	-318.2	-326.0	-333.8	-341.6	-349.4	-357.2	-365.0

Tab.10 Dropping temperatures on tendons for beams with four tendons in pre-tensioning

Cases	D1	D2	D3	D4	D5	D6	D7	D8	D9	D10	D11
t_{11}, t_{12}	-279.2	-287.2	-295.1	-303.1	-311.0	-319.0	-326.9	-334.9	-342.8	-350.8	-358.7
t_{21}, t_{22}	-292.0	-300.1	-308.2	-316.3	-324.4	-332.5	-340.6	-348.7	-356.9	-365.0	-373.1
t_{31}, t_{32}	-300.7	-308.8	-317.0	-325.2	-333.3	-341.5	-349.6	-357.8	-366.0	-374.1	-382.3
t_{41}, t_{42}	-304.7	-312.8	-320.9	-329.0	-337.1	-345.2	-353.3	-361.4	-369.5	-377.6	-385.7

Contours of displacements and stresses are depicted in Fig.11 for non-prestressed beams under gravity and two prestressed beams in pre-tensioning under the case C6, where P=0kN. It is obvious that compared with the non-prestressed beams (Fig.11a), the y-axial displacement UY at mid span changes from the downward to upward, and the warping stress on bottom flange changes from tension to compression after being prestressed, which results in the vanish of neutral axis in the range of cross section. So the external force P needs to overcome the prestressed force first in the later loading period, which largely improves the loading capacity of beam.

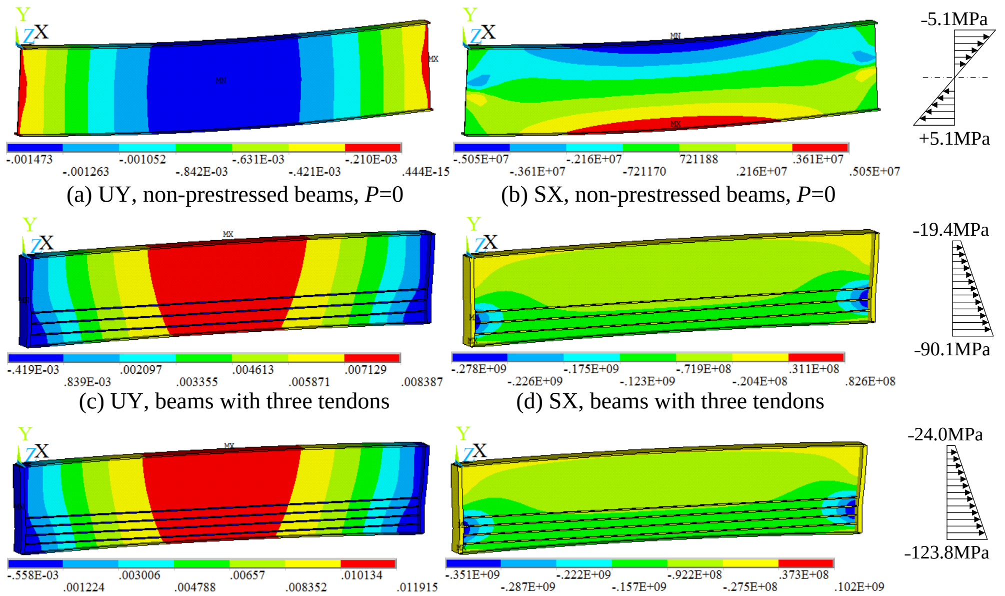

(a) UY, non-prestressed beams, P=0 (b) SX, non-prestressed beams, P=0

(c) UY, beams with three tendons (d) SX, beams with three tendons

(e) UY, beams with four tendons (f) SX, beams with four tendons

Fig.11 Contours of displacements UY and warping stresses SX for non-prestressed beams under gravity and two prestressed beams in pre-tensioning under the case C6 (unit: m, Pa).

Comparisons of displacements obtained from FEA and the proposed method are tabulated in Tab.11 and Tab.12 respectively for two prestressed beams in pre-tensioning. It is seen that the proposed method provides a high accuracy in calculating the y-axial displacements with the RE less than 1% for all cases. So the proposed method has a strong ability in solving the vertical displacements for prestressed beams in pre-tensioning.

Tab.11 Comparisons between FEA and the proposed method for the *y*-axial displacement of beams with three tendons in pre-tensioning (unit: mm, direction: upwards)

Cases	C1	C2	C3	C4	C5	C6	C7	C8	C9	C10	C11
FEA	6.99	7.23	7.46	7.70	7.93	8.17	8.40	8.64	8.87	9.11	9.34
Eq.(19)	7.06	7.30	7.53	7.77	8.00	8.24	8.47	8.71	8.94	9.18	9.41
RE (%)	0.95	0.93	0.91	0.89	0.87	0.85	0.83	0.81	0.79	0.77	0.75

Tab.12 Comparisons between FEA and the proposed method for the *y*-axial displacement of beams with four tendons in pre-tensioning (unit: mm, direction: upwards)

Cases	D1	D2	D3	D4	D5	D6	D7	D8	D9	D10	D11
FEA	10.06	10.37	10.68	11.00	11.31	11.63	11.94	12.26	12.57	12.89	13.20
Eq.(19)	10.12	10.43	10.75	11.06	11.37	11.69	12.00	12.31	12.62	12.94	13.25
RE (%)	0.63	0.60	0.57	0.55	0.52	0.49	0.46	0.44	0.41	0.38	0.35

Similarly, the warping stresses on flanges at mid span, obtained from FEA and the proposed method, are compared in Tab.13 and Tab.14 for two prestressed beams in pre-tensioning. It is seen that the proposed method (Eq.(20)) gives an acceptable results in calculating the warping stresses with all REs being less than 7%. So the proposed method is capable of estimating the warping stresses on flanges for beams externally prestressed with multi-tendons in pre-tensioning.

Tab.13 Comparisons between FEA and the proposed method for warping stresses on flanges for beams with three tendons in pre-tensioning (σ_u: stress on top flange, σ_d: stress on bottom flange, unit: MPa)

Cases		C1	C2	C3	C4	C5	C6	C7	C8	C9	C10	C11
	FEA	-17.72	-18.06	-18.41	-18.75	-19.09	-19.44	-19.78	-20.12	-20.47	-20.81	-21.15
σ_u	Eq.(20)	-18.99	-19.33	-19.66	-20.00	-20.33	-20.66	-21.00	-21.33	-21.67	-22.00	-22.34
	RE (%)	6.73	6.56	6.39	6.23	6.08	5.94	5.80	5.67	5.54	5.42	5.31
	FEA	-78.40	-80.73	-83.06	-85.39	-87.72	-90.05	-92.37	-94.70	-97.03	-99.36	-101.7
σ_d	Eq.(20)	-77.25	-79.59	-81.93	-84.27	-86.61	-88.95	-91.29	-93.63	-95.97	-98.31	-100.6
	RE (%)	1.47	1.41	1.36	1.31	1.26	1.22	1.17	1.14	1.10	1.06	1.03

Tab.14 Comparisons between FEA and the proposed method for warping stresses on flanges for beams with four tendons in pre-tensioning (σ_u: stress on top flange, σ_d: stress on bottom flange, unit: MPa)

Cases		D1	D2	D3	D4	D5	D6	D7	D8	D9	D10	D11
	FEA	-21.74	-22.19	-22.65	-23.10	-23.56	-24.01	-24.46	-24.92	-25.37	-25.82	-26.27
σ_u	Eq.(20)	-22.90	-23.35	-23.80	-24.24	-24.69	-25.14	-25.60	-26.05	-26.50	-26.95	-27.40
	RE (%)	5.07	4.94	4.82	4.71	4.61	4.51	4.42	4.33	4.25	4.18	4.11
	FEA	-108.3	-111.4	-114.5	-117.6	-120.7	-123.8	-126.9	-130.0	-133.1	-136.2	-139.4
σ_d	Eq.(20)	-107.2	-110.3	-113.5	-116.6	-119.7	-122.8	-125.9	-129.0	-132.1	-135.2	-138.4
	RE (%)	0.96	0.92	0.89	0.86	0.84	0.81	0.79	0.77	0.75	0.73	0.71

5.3. The increase in tendon force

Based on the initial prestressed forces in the cases C6 and D6, verifications on the increases in sub-tendon forces are performed under a series of forces P in Tab.15 and Tab.16 for the two prestressed beams, where $S_{\Delta j1}$ is the increase in the sub-tendon T_{j1} (j=1,2,3,4) and $S_{\Delta j1}$=$S_{\Delta j2}$ due to the symmetry of sub-tendons. It is seen that almost all REs are less than 10% and those for sub-tendons with larger eccentricities are much smaller. Besides, results obtained from the proposed method (Eq.(21)) are larger than those from FEA, which means the proposed method is conservative in estimating the increase in tendon force.

Additionally, the influences of meshing size (MS) in FEA on the above REs are analyzed in Fig.12 for two prestressed beams respectively, where P=10000kN. It is seen that the REs reduce slightly and tend to be stable for the gradually refined meshing gird for both prestressed beams. Therefore, the proposed method (Eq.(21)) can be applied to calculate the increase in tendon force.

Tab.15 Comparisons between FEA and the proposed method for the increase in sub-tendons for beams with three tendons (unit: kN)

	P	1000	2000	3000	4000	5000	6000	7000	8000	9000	10000
$S_{\Delta 11}$ $S_{\Delta 12}$	FEA	17.7	36.0	54.3	72.5	90.7	108.7	126.8	144.7	162.6	180.4
	Eq.(21)	19.6	39.2	58.8	78.3	97.9	117.5	137.1	156.7	176.3	195.8
	RE (%)	9.62	8.09	7.58	7.45	7.37	7.49	7.50	7.64	7.75	7.88
$S_{\Delta 21}$ $S_{\Delta 22}$	FEA	38.9	79.3	119.6	159.9	200.1	240.2	280.3	320.3	360.2	400.1
	Eq.(21)	42.5	85.0	127.5	170.0	212.5	255.0	297.5	340.0	382.5	425.0
	RE (%)	8.47	6.70	6.19	5.94	5.83	5.80	5.78	5.79	5.82	5.85
$S_{\Delta 31}$ $S_{\Delta 32}$	FEA	61.3	125.2	188.9	252.6	316.3	379.8	443.3	506.7	570.1	633.4
	Eq.(21)	65.4	130.8	196.2	261.6	327.1	392.5	457.9	523.3	588.7	654.1
	RE (%)	6.28	4.30	3.74	3.46	3.29	3.23	3.18	3.17	3.16	3.17

Tab.16 Comparisons between FEA and the proposed method for the increase in sub-tendons for beams with four tendons (unit: kN)

	P	1000	2000	3000	4000	5000	6000	7000	8000	9000	10000
$S_{\Delta 11}$ $S_{\Delta 12}$	FEA	12.4	25.2	38.0	50.8	63.4	76.1	88.6	101.1	113.6	125.9
	Eq.(21)	13.8	27.7	41.5	55.4	69.2	83.1	96.9	110.8	124.6	138.5
	RE (%)	10.45	9.01	8.53	8.29	8.43	8.41	8.60	8.74	8.85	9.08
$S_{\Delta 21}$ $S_{\Delta 22}$	FEA	28.9	59.0	89.0	119.0	148.9	178.7	208.5	238.2	267.8	297.4
	Eq.(21)	32.0	64.0	96.0	127.9	159.9	191.9	223.9	255.9	287.9	319.8
	RE (%)	9.64	7.77	7.24	6.98	6.89	6.88	6.87	6.91	6.97	7.01
$S_{\Delta 31}$ $S_{\Delta 32}$	FEA	46.1	94.0	141.9	189.7	237.4	285.1	332.7	380.2	427.7	475.1
	Eq.(21)	50.1	100.2	150.4	200.5	250.6	300.7	350.8	401.0	451.1	501.2
	RE (%)	8.02	6.22	5.63	5.38	5.27	5.19	5.17	5.18	5.18	5.21
$S_{\Delta 41}$ $S_{\Delta 42}$	FEA	64.4	131.5	198.5	265.5	332.4	399.2	466.0	532.7	599.3	665.9
	Eq.(21)	68.3	136.5	204.8	273.0	341.3	409.5	477.8	546.0	614.3	682.6
	RE (%)	5.65	3.67	3.06	2.75	2.60	2.52	2.47	2.44	2.44	2.44

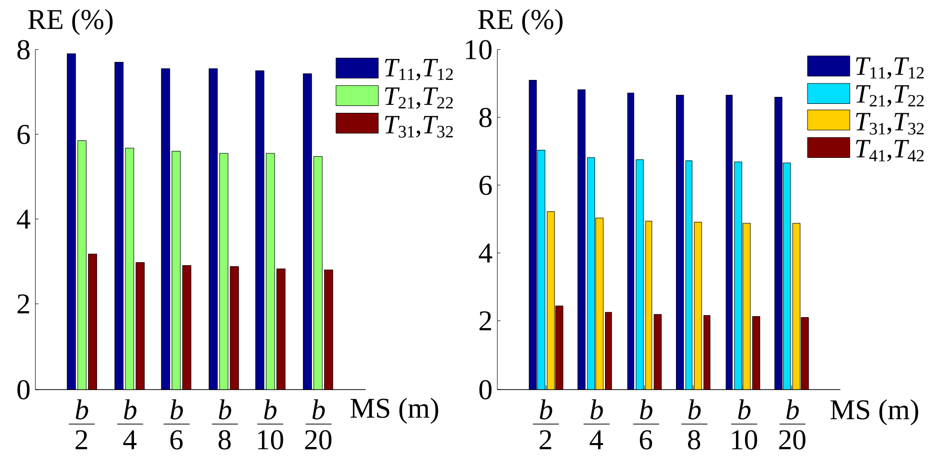

(a) beams with three tendons (b) beams with four tendons

Fig.12 Relative errors (RE) versus the meshing size in FEA for the increases in sub-tendon force for two prestressed beams (b is the width of flanges, b=1.5m)

6. Parametric study

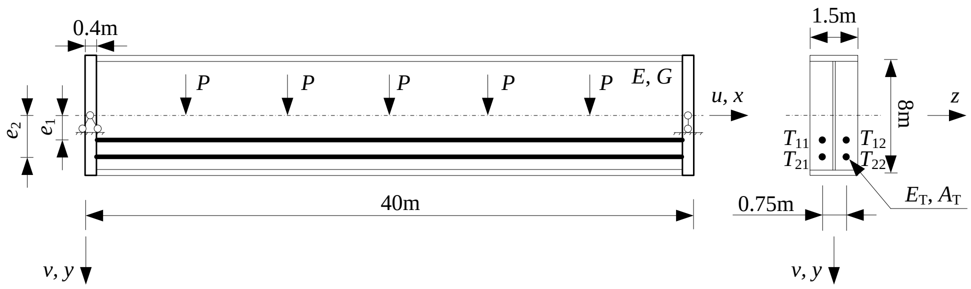

Fig.13 Deep I-shaped beams prestressed with two straight tendons

In order to investigate the effects of tendon force and eccentricity on the flexural behavior of beams, a deep I-shaped beam externally prestressed with two straight tendons are analyzed under five evenly-distributed forces P (P=10000kN) for both post- and pre-tensioning processes, in which the measurements and beam self weight refer to Section 5. The Young's elastic module E and Poisson's ratio v are 210GPa and 0.3 respectively. For the sub-tendon T_{ij}, the tendon force and eccentricity are S_{ij} and e_i, in which S_{11}=S_{12} and S_{21}=S_{22} due to the symmetry of sub-tendons. Two ratios ρ_S and ρ_e are herein defined by ρ_S=S_{21}/S_{11} and $\rho_e=|e_2\text{-}e_1|/h$, respectively. The cross-sectional area and elastic module of the sub-tendons T_{ij} are uniform A_{Ti} and E_{Ti} (i=1, 2), respectively. The tensioning capacity f_{ptk} of sub-tendons is uniform 1625MPa.

Relations between the location of neutral axis and the tendon forces and eccentricities are analyzed in Fig.14 for both post- and pre-tensioning in terms of two ratios ρ_S and ρ_e, respectively.

For post-tensioning in Fig.14a, the distance e_N increases non-linearly in terms of the tendon force and eccentricity with a increasing rate, and those with larger ratios ρ_S or ρ_e are much larger. While for pre-tensioning in Fig.14b, the distance e_N varies in the form of a logarithm-shaped function. The curves with larger ratios ρ_S and ρ_e have a smaller absolute value of e_N, resulting in a larger difference for stresses between top and bottom flanges, so that it needs a larger external force P to make the warping stresses on bottom flange change from compression to tension.

Besides, the effects of tendon eccentricity on the increases in sub-tendon forces ($S_{\Delta 21}$, $S_{\Delta 11}$) and strains ($\varepsilon_{\Delta 21}$, $\varepsilon_{\Delta 11}$) are analyzed in Fig.15 in terms of the tensile rigidity K_{Ti} of sub-tendons T_{ij} (j=1, 2) and the ratio ρ_e respectively, where $K_{Ti}=E_{Ti}A_{Ti}$ and K_{T1}=0.068GA.

As shown in Fig.15a, the ratio $S_{\Delta 21}/S_{\Delta 11}$ reduces non-linearly in terms of the eccentricity e_1 with a decreasing rate, and those with larger ρ_e and K_{T2} are much larger. Similar variability happens to the tendon strains in Fig.15b. However, it almost makes no difference between the cases with '$K_{T2}=K_{T1}$' and those with '$K_{T2}=1.6K_{T1}$'. This infers that the ratio $\varepsilon_{\Delta 21}/\varepsilon_{\Delta 11}$ almost has nothing to do with the ratio K_{T2}/K_{T1}. Furthermore, considering the equation '$K_{Ti}=E_{Ti}A_{Ti}$', we know that the changes on the module E_{Ti} or area A_{Ti} will not affect the ratio $\varepsilon_{\Delta 21}/\varepsilon_{\Delta 11}$.

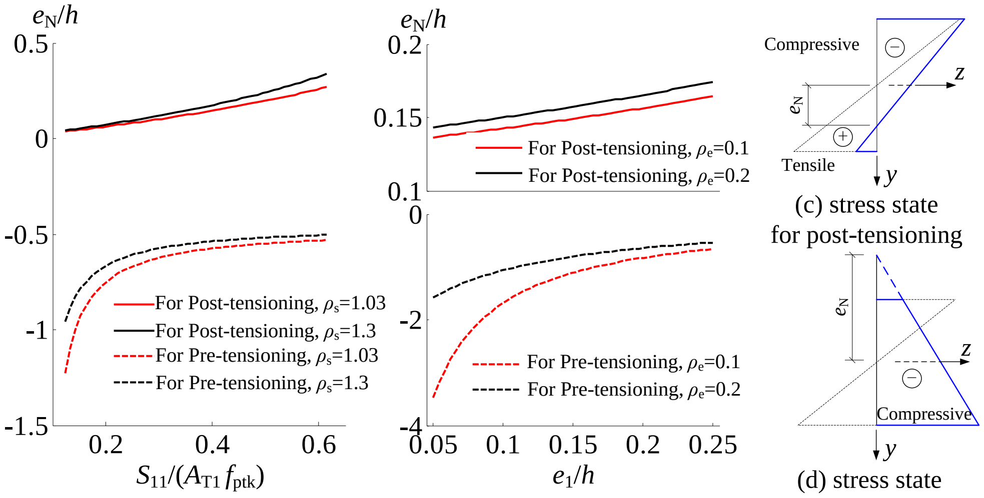

(a) e_N versus S_{11} under ρ_e=0.2 (b) e_N versus e_1 under ρ_s=1.3

Fig.14 Relations between the location of neutral axis and the tendon forces and eccentricities (A_{T1}=0.01m^2)

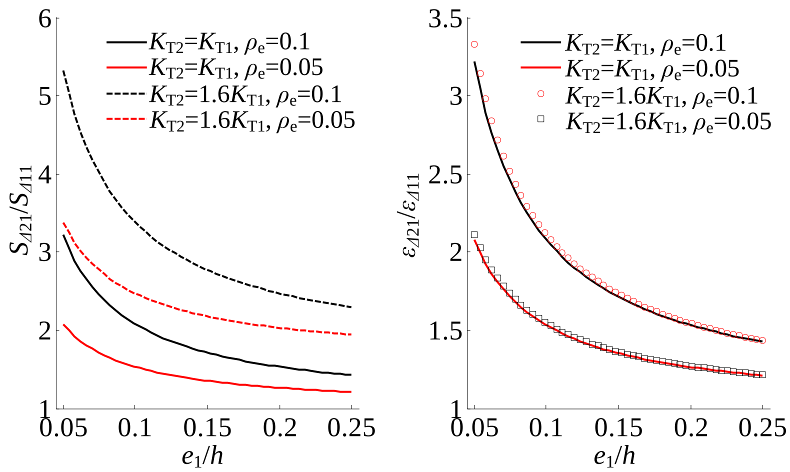

(a) tendon force (b) tendon strain

Fig.15 The ratios of the increases in sub-tendon forces and strains in terms of the eccentricity e_1 (K_{T1}=0.068*GA*)

Conclusion

In this paper, the flexural behavior of deep beam prestressed with straight multi-tendons is investigated under concentrated forces for both post- and pre- tensioning processes.

Main conclusions are drawn as follows

(1) The proposed method is capable of estimating the vertical displacements and warping stresses on flanges for beams prestressed with multi-tendons for both post- and pre- tensioning, which has been well verified by FEA.

(2) For prestressed beams in loading period in pre-tensioning, the proposed method offers an acceptable and conservative estimation on the increase in tendon force, and the deviation with FEA decreases with the gradually refined meshing gird in FEA model.

(3) Prestressed beams with larger tendon forces or distances between tendons display a more significant prestressed effect for both post- and pre- tensioning, resulting in a larger difference for stresses between the top and bottom flanges. Besides, the ratio of tensile rigidities between the top and bottom sub-tendons almost makes no change to that of the increases in sub-tendon strains.

Future work are needed for (1) beams prestressed with draped multi-tendons; (2) the local stability of anchorages; (3) the relaxation of tendons.

Acknowledgements

This work was supported by the National Natural Science Foundation of China (NSFC) [grant number: 51378289 and 51678339].

References

[1] A. Dall'Asta, A. Zona, Finite element model for externally prestressed composite beams with deformable connection, J. Struct. Eng. 131 (2005) 706-714.

[2] S.M. Chen, X.D. Wang, Y.L. Jia, A comparative study of continuous steel–concrete composite beams prestressed with external tendons: experimental investigation, J. Constr. Steel Res. 65 (2009) 1480–1489.

[3] J.G. Nie, C.S. Cai, T.R. Zhou, Y. Li, Experimental and analytical study of prestressed steel–concrete composite beams considering slip effect, J. Struct. Eng. 133 (2007) 530-540.

[4] T.J. Lou, S.M.R. Lopes, A.V. Lopes, Numerical modeling of externally prestressed steel -concrete composite beams, J. Constr. Steel Res. 121 (2016) 229–236.

[5] J.G. Nie, M.X. Tao, C.S. Cai, S.J. Li, Deformation analysis of prestressed continuous steel -concrete composite beams, J. Struct. Eng. 135 (2009) 1377-1389.

[6] A. El-Zohairy, H. Salim, H. Shaaban, S. Mustafa, A. El-Shihy, Finite-element modeling of externally posttensioned composite beams, J. Bridge Eng. 20 (2015) 04015018.

[7] B.M. Ayyub, Y.G. Sohn, H. Saadatmanesh, Prestressed composite girders under positive moment, J. Struct. Eng. 116 (1990) 2931-2951.

[8] B.M. Ayyub, Y.G. Sohn, H. Saadatmanesh, Prestressed composite girders. II: analytical study for negative moment, J. Struct. Eng. 118 (1992) 2763-2782.

[9] K.H. Tan, C.K. Ng, Effects of deviators and tendon configuration on behavior of externally prestressed beams, ACI Struct. J. 94 (1997) 13-22.

[10] M. Harajli, N. Khairallah, H. Nassif, Externally prestressed members: evaluation of second -order effects, J. Struct. Eng. 125 (1999) 1151-1161.

[11] F.M. Alkhairi, A.E. Naaman, Analysis of beams prestressed with unbonded internal or external tendons. J. Struct. Eng. 119 (1993) 2680-2700.

[12] T.J. Lou, S.M.R. Lopes, A.V. Lopes, Nonlinear and time-dependent analysis of continuous unbonded prestressed concrete beams, Comput. Struct. 119 (2013) 166-176.

[13] F. Biondini, F. Bontempi, D.M. Frangopol, P.G. Malerba, Reliability of material and geometrically non-linear reinforced and prestressed concrete structures, Comput. Struct. 82 (2004) 1021-1031.

[14] A. Miyamoto, K. Tei, H. Nakamura, J.W. Bull, Behavior of prestressed beam strengthened with external tendons, J. Struct. Eng. 126 (2000) 1033-1044.

[15] W. Lorenc, W. Kubica, Behavior of composite beams prestressed with external tendons: experimental study, J. Constr. Steel Res. 62 (2006) 1353–1366.

[16] A. Zona, L. Ragni, A. Dall'Asta, Simplified method for the analysis of externally prestressed steel–concrete composite beams, J. Constr. Steel Res. 65 (2009) 308–313.

[17] N. Zhang, C.C. Fu, Experimental and theoretical studies on composite steel–concrete box beams with external tendons, Eng. Struct. 31 (2009) 275–283.

[18] K.H. Tan, K. Tong, C.Y. Tang, Direct strut-and-tie model for prestressed deep beams, J. Struct. Eng. 127 (2001) 1076-1084.

[19] G.L. Wang, S.P. Meng, Modified strut-and-tie model for prestressed concrete deep beams, Eng. Struct. 30 (2008) 3489–3496.

[20] T.H. Kim, J.H. Cheon, H.M. Shin. Evaluation of behavior and strength of prestressed concrete deep beams using nonlinear analysis, Comput. Concrete 9 (2012) 63-79.

[21] B. Belletti, A. Gasperi. Behavior of Prestressed Steel Beams, J. Struct. Eng. 136 (2010) 1131-1139.

[22] S.Y. Park, T.W. Kim, K.W.S. Kim, S.N. Hong. Flexural behavior of steel I-beam prestressed with externally unbonded tendon, J. Constr. Steel Res. 66 (2010) 125–132.

[23] S.Y. Park, T.W. Kim, S.N. Hong. Flexural behavior of continuous steel girder with external post-tensioning and section enhancement, J. Constr. Steel Res. 66 (2010) 248–255.

[24] G.T. Michaltsos, I.G. Raftoyiannis, The influence of prestressing on the twisting phenomenon of beams, Arch. Appl. Mech. 82 (2012) 1531–1540.

[25] S.P. Timoshenko. Strength of Materials (Part I): Elementary Theory and Problems. Lancaster, 1955.

[26] American Institute of Steel Construction (AISC). Specification for structural steel buildings; 2010.